



Framework for developing IDF curves using satellite precipitation: a case study using GPM-IMERG V6 data

Kasi Venkatesh^{1,2} · Rathinasamy Maheswaran¹ · Jarajapu Devacharan¹

Received: 29 January 2021 / Accepted: 20 September 2021 / Published online: 2 October 2021
© The Author(s), under exclusive licence to Springer-Verlag GmbH Germany, part of Springer Nature 2021

Abstract

With the availability of satellite-based precipitation products, it is pertinent to develop methods to use these data products to design hydraulic structures. The satellite precipitation products play a vital role in ungauged locations or when information is required on a catchment scale. Before such applications, the accuracy and uncertainty associated with the products have to be investigated. In this study, we develop a framework that includes bias correction for the development of robust IDF curves. The framework is applied to a small region in the southeastern part of India, and the IDF curves were evaluated using the gauge data at nine locations. This study compares Intensity Duration Frequency (IDF) curves using the recent precipitation product Global Precipitation Measurement (GPM-IMERG V6) with ground-based gauge data. Results show that the spatial correlation between the satellite IDF and the gauge-based IDF improves significantly after bias correction, and the value is as high as 0.75 for 2–10 year return period. The bias between the satellite IDF and gauge IDF is low in the north part of the study region and is high in the southeastern part, prone to extreme rainfall. Further, a significant percentage of the satellite-based IDFs (with and without bias correction) lie inside the confidence interval of the gauge-based data. Thus, GPM V6 data have the potential to be used as an alternate data source for IDF generation in developing countries.

Keywords Satellite-based precipitation · Global precipitation measurement (GPM) · Intensity frequency duration (IDF) curve

Introduction

Floods are among the most common natural hazards resulting in loss of lives and infrastructure (Maheswaran and Khosa 2013, 2012; Kasi et al. 2020a). In the past few decades, almost 20,000 people are killed over the entire globe, and almost 58 million people are affected due to severe floods (Cross 2010; WDR 2018; Yeditha et al. 2020; Kumar et al. 2021). To minimize flood risk and reduce the loss of life and property accurate estimate of design floods is required while designing hydraulic structures. Intensity Duration Frequency (IDF) relationships are generally developed to estimate the design floods (Watt and Marsalek 2013). The derived IDF curves are generally used for

hydrological design purposes and verdict support evidence in flood risk and water resources management. IDF curves are the mathematical relationship between the rainfall intensity ‘I’ versus duration of time ‘D’ in hours over the various return period (T) in years (Overeem et al. 2008; Dong et al. 2013; Vivekanandan 2013; Bhatt and Ahmed 2014; Wayal and Menon 2014; Tfwala et al. 2017). IDF curves are developed using historical annual maximum series (AMS) of rainfall data which were then best fitted with appropriate probability distribution to estimate the rainfall intensities over the given storm duration and return period (Overeem et al. 2008; Cheng et al. 2014). The developed IDF curves assume that the occurrences and distribution of precipitation patterns are spatially similar and remain unchanged throughout the lifespan of the infrastructure (Cheng et al. 2014; Agarwal et al. 2018, 2020; Setti et al. 2018).

Several studies have investigated the parametric formulation of IDF curves relationships and estimation of the parameters in the past. Some of the significant and critical works include Chow et al. 1988; Koutsoyiannis et al. 1998 and Hosking and Wallis, 1993 wherein the latter have introduced

✉ Rathinasamy Maheswaran
maheswaran27@yahoo.co.in

¹ Department of Civil Engineering, MVGR College of Engg, Vizianagaram 535005, India

² School of Infrastructure, Indian Institute of Technology Bhubaneswar, Bhubaneswar, India

L-moments-based estimation uses the probability-weighted moments (Greenwood et al. 1979) in developing IDF curves. Koutsoyiannis et al. (1998) implemented regionalization methods such as the Index Flood method to develop IDF curves. Stewart et al. (1999) developed various rainfall contour maps to design rainfall depths for various return periods and durations. Bairwa et al. (2016) developed IDF curves-based probability weighted moments and scaling laws for urban clusters in India.

Developing robust IDF curves requires accurate and reliable precipitation datasets. One of the significant sources for real-time monitoring precipitation data is the ground-based observation gauge data. For many decades, ground-based gauge datasets were the primary sources that were used for developing IDF curves. The developed IDF Curves using ground-based gauge datasets give reliable results (Zope et al. 2016; Ombadi et al. 2018). However, due to extensive cost involvement for installing and maintaining, the rain gauge distribution is scarce (Endreny and Imbeah, 2009; Marra et al. 2017; Ombadi et al. 2018; Agarwal et al. 2020). As an alternative to ground-based gauge measurements, satellite-based precipitation products have been used for developing IDF curves. The main advantages of the satellite-based precipitation products are (i) real-time monitoring/capturing dynamics and variability of extreme rainfall events that are not signified by a rain gauge. (Endreny and Imbeah 2009; Aghakouchak A et al. 2011; Al-hassoun 2011; Hisham Abd El-Kareem El-Dardiry 2014; Marra et al. 2017; Ombadi et al. 2018; Noor et al. 2021) (ii) provides high spatial and temporal resolution precipitation datasets (Amitai et al. 2012; Tapiador et al. 2012; Chen et al. 2013; Marra et al. 2016; Panziera et al. 2016; Raj et al. 2021). In the past, the utility of several precipitation products such as Tropical Rainfall Measuring Mission (TRMM) (Endreny and Imbeah 2009), Precipitation Estimation from Remotely Sensed Information Using Artificial Neural Networks (PERSIANN) (Ombadi et al. 2018), Climate Prediction Center (CPC) MORPHING technique (CMORPH) (Ombadi et al. 2018), have been successfully used in developing IDF. For example, Endreny and Imbeah (2009) used Tropical Rainfall Measuring Mission (TRMM) precipitation product datasets over the Ghana region for developing IDF curves, Endreny and Imbeah 2009 combined TRMM precipitation product datasets with ground-based precipitation data to develop IDF curves. Similarly, Awadallah et al. 2011 examined TRMM precipitation product datasets and ground-based precipitation datasets to construct IDF curves over the Northwestern Angola region. Recently, Gado et al. (2017) developed IDF curves for two basins in Colorado and California region by combining ungauged sites and PERSIANN-CDR datasets. Further, Marra et al. (2017) develop and compared derived IDF curves using Climate Prediction Center morphing (CMORPH) and radar data over the eastern Mediterranean

region. Overall, these studies show that the satellite-retrieved precipitation product can be an alternative source to develop IDF curves, particularly in sparse gauged sites. Indeed, there has been significant work in developing IDF curves to evaluate and implement satellite precipitation.

With the advent of GPM-era satellites (Huffman et al. 2015), GPM-based rainfall estimates (v3, v4, v5) have been shown to be better than TRMM (Tan et al. 2019; Tang et al. 2020). More recently, a new version of GPM-IMERG, V6 is made available wherein the algorithm can fuse the data collected during the TRMM era (2000–2014) with the precipitation estimates collected during the GPM era, thereby IMERG data is now available from June 2000 (<https://pmm.nasa.gov/dataaccess/downloads/GPM>). Studies have shown that the IMERG v6 can be reliably used for hydrologic application (Tang et al. 2016; Zhang et al. 2019; Le et al. 2020; Ahmed et al. 2020). Several studies in various geographical areas demonstrated the accuracy of the GPM IMERG. For example, Tan and Duan 2017 revealed a good correlation found with GPM IMERG daily and monthly scales with rain gauge data. Similarly, Wang et al. 2019 mainly found that GPM IMERG can detect better moderate and heavy rainfall and better correlate with daily scale. Chen et al. 2018 assessed the performance of TRMM 3B42 (v7) and IMERG (v5), and results found that IMERG datasets were highly correlated at monthly and annual scales with the rain gauge observations.

The studies mentioned above have explored the reliability and accuracy of the IMERG v6 product, but no studies are investigating its applicability for the IDF curve generation. Therefore, this research study's principal goal is to provide a suitable methodological framework for constructing IDF curves using the GPM-IMERG v6 product and investigate its accuracy by comparing it with the rain gauge-based estimates. We have chosen the Vizianagaram district in the southern part of India as a testbed for this purpose. The study area is located in the tropical region and is characterized by a monsoonal climate with regular cyclones.

The rest of the paper is arranged in the following manner. Section 2 provides information about the study area and data sets used. Section 3 explains the methodology adopted in this study. The results are discussed in Sect. 4, and Sect. 5 provides overall concluding remarks from the study.

Study area and data used

Study area

Vizianagaram district is considered as the testbed for this study as the ground gauge data is available in sufficient data length. It is located on the Southeastern part of the Indian subcontinent (see Fig. 1) and is bounded by the Bay

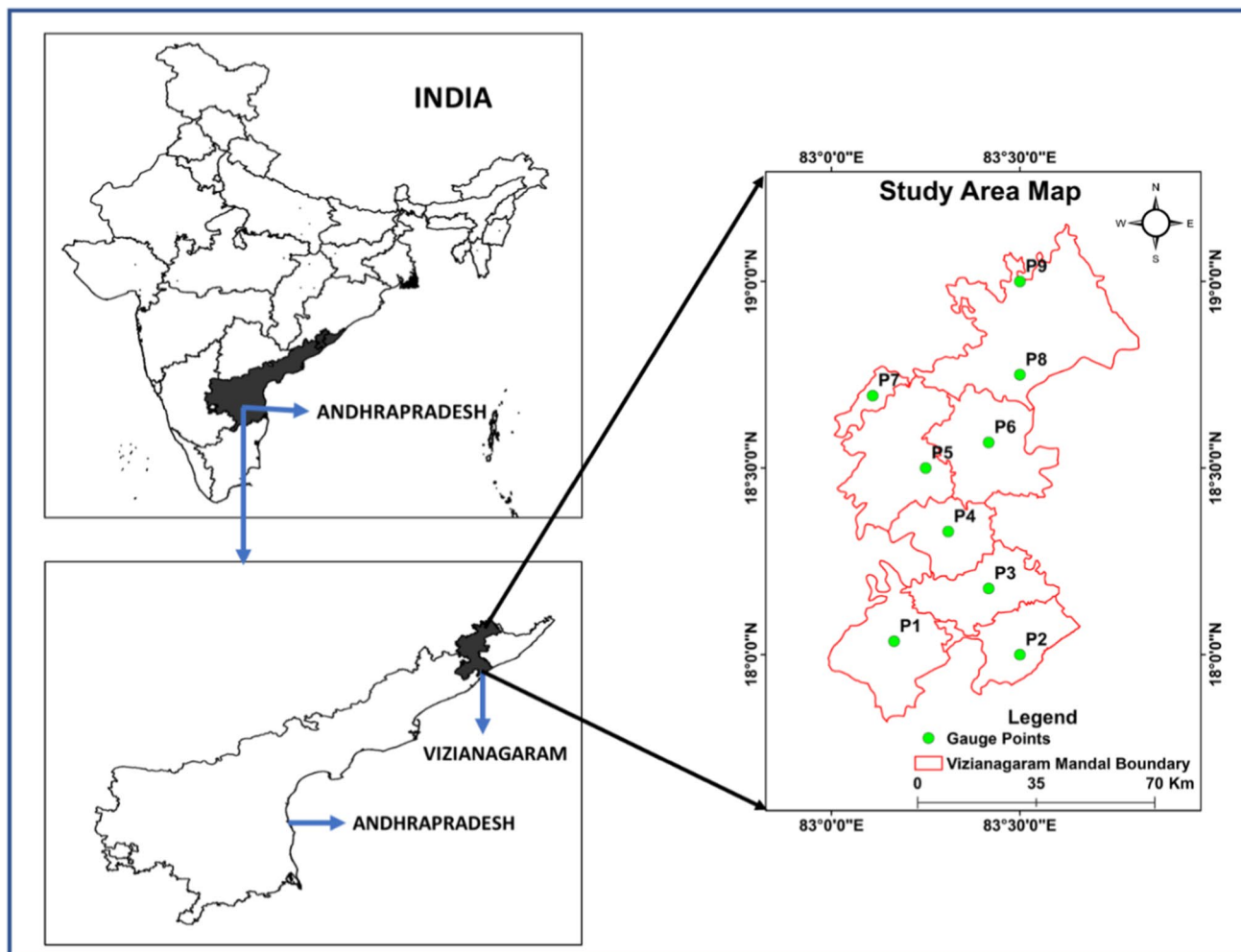


Fig. 1 Geographical location of the study area. The right bottom panel shows the study area bounded in andhra pradesh state and the left panel show the index map of the study area of the entire vizianagaram district covered with nine gauge points

Table 1 General meteorological characteristics in Vizianagaram District, South India during the period from 2000 to 2018

S. No	Parameters	Value
1	Daily maximum precipitation (mm)	218.36
2	Average annual precipitation (mm)	1097
3	Maximum temperature °C	31.1
4	Minimum temperature °C	27.3
5	Average relative humidity (%)	75

of Bengal on the South East (Pinninti et al. 2021). The geographical area of the Vizianagaram district is about 6539 sq. km, and the latitude and longitude of this area are $18.12N^0$ and $83.42E^0$, respectively (Kasi et al. 2020b).

The general meteorological conditions prevailing over the study area are shown in Table 1.

Data used

Ground-based rain gauge data

The observed rain gauge data was obtained from the Andhra Pradesh State Government, Central Planning Office, Vizianagaram. Andhra Pradesh State Government has installed a rain gauge in each Mandal (a subdivision in the district). The same is maintained by the Andhra Pradesh State Development Planning Society (APSDPS). For this study, we have collected the Vizianagaram Central Planning Office data for the period from 2000 to 2019 at nine locations spread across the district. The locations of the rain gauge stations are shown in Fig. 1.

Global precipitation measurements (GPM) data

Global Precipitation Measurement (GPM) is a collaboration mission organized by the National Aeronautics and Space Administration (NASA) and Japan Aerospace Exploration Agency (JAXA) (Huffman et al. 2013; Ning et al. 2016; Omranian and Sharif 2018). It estimates global precipitation and provides improved weather systems and information on extreme weather events. It is an international satellite mission that provides precipitation estimates for every three hours interval over the globe (Omranian and Sharif 2018).

GPM is much more improved than its predecessor, TRMM, in detecting the light and solid precipitation, which became possible by using two different instruments, i.e., the Dual-frequency Precipitation Radar (DPR) and GPM Microwave Imager (GMI) (Yang et al. 2014; Yong et al. 2015; Zhang et al. 2016). The GPM Microwave Imager (GMI) is a type of conical scanning radiometer, whereas the Dual-Frequency Precipitation Radar (DPR) consists of two bands, i.e., Ka-band and Ku-band. The GMI radiometer frequency ranges from about 10 to 183 GHz and the DPR at Ka-band frequency range about 35.5 GHz, and the Ku band frequency coverage about 13.6 GHz (Omranian and Sharif 2018). The DPR offers measurements spread out at nearly 5 km over 245 km and 120 km wide swaths for Ku band and ka-band (Khan and Maggioni 2019). The Integrated Multi-Satellite Retrievals for GPM used the algorithm to investigate and revise rainfall estimates utilizing all passive-microwave devices present in the GPM constellation (Grecu et al. 2016; Naud et al. 2018; Wang et al. 2019). GPM microwave imager has more frequency channels than TRMM, and the precipitation radar is advanced (Huffman et al. 2015). More significantly, spatial coverage (60°S–60°N) and the spatiotemporal resolution (30 min and $(0.1^\circ \times 0.1^\circ)$) have been improved compared to the previous SPPs. The GPM team has developed GPM-IMERG precipitation products using the IMERG algorithm that combines three SPPs features, including PERSIANN-CDR, CMORPH, and TRMM. Three types of IMERG products are made available: early run, late run and final run with a latency period of 4 h, 14 h and 3.5 months. The first two products are useful in real-time applications, whereas the latter can be used for water balance studies. All these products are available at $0.1^\circ \times 0.1^\circ$ spatial resolution over the fully global domain.

Presently, IMERG is at its Version 06 stage (<https://gpm.nasa.gov/missions/two-decades-imerg-resources>). The new thing in Version 06 IMERG is that the algorithm combines the data collected during the TRMM era (2000–2014) with the precipitation estimates collected during the GPM era. Due to this, IMERG is now available from June 2000 (<https://pmm.nasa.gov/dataaccess/downloads/gpm>). The "Final run" of IMERG combines the GPCC Monitoring product, the V8 Full Data Analysis, for most of the time

(currently 1998–2019). This study used the GPM-IMERG v6 final run precipitation product from June 2000 to Jun 2019 for the study. Further, the GPM-IMERG v6 data was downloaded at grid locations that are near the gauge locations.

We have derived the 2-day and 3-day precipitation from the available daily satellite-based precipitation (GPM) product and gauge precipitation data for the IDF curve generation.

Methodology

In this section, the methodology used for developing IDF curves using GPM data is presented. Here, apart from using the satellite data for IDF generation, it is also intended to investigate the effect of using the bias-corrected product. For this purpose, we use the strategy proposed by (Ombadi et al. 2018). The overall methodology is represented in the form of a flow chart shown in Fig. 2.

Homogeneity test

There is always a question of whether the underlying probability distribution remains constant or not, especially in hydro climatological studies (Kisi 2015; Dash et al. 2017; Agarwal et al. 2017). The changes can be attributed to several causes. However, for the present analysis, the assumption of stationarity must be verified. The homogeneity test is essential for assessing the extreme annual rainfall data and would provide confidence in the datasets for development of IDF curves.

The homogeneity test can be done using a parametric and nonparametric test. The analyzed variables are assumed to be normally distributed in the parametric test, whereas the nonparametric methods do not make any assumptions. Many statistical approaches can be applied to evaluate the homogeneity of the time series data. Of the different methods, in this study, nonparametric homogeneity test, Pettit test is used because, according to the earlier investigation, proved to be most reliable in detecting the break or change points in the time series data (Wijngaard et al. 2003; Costa and Soares 2009; Hurtado et al. 2020).

Pettit test

Pettit test is a nonparametric homogeneity test that is considered more sensitive to detect the break point in the middle of the time series (Pettit 1979; García-Marín et al. 2020). The Pettit test uses the version of Mann–Whitney statistic $U_{i,n}$, in

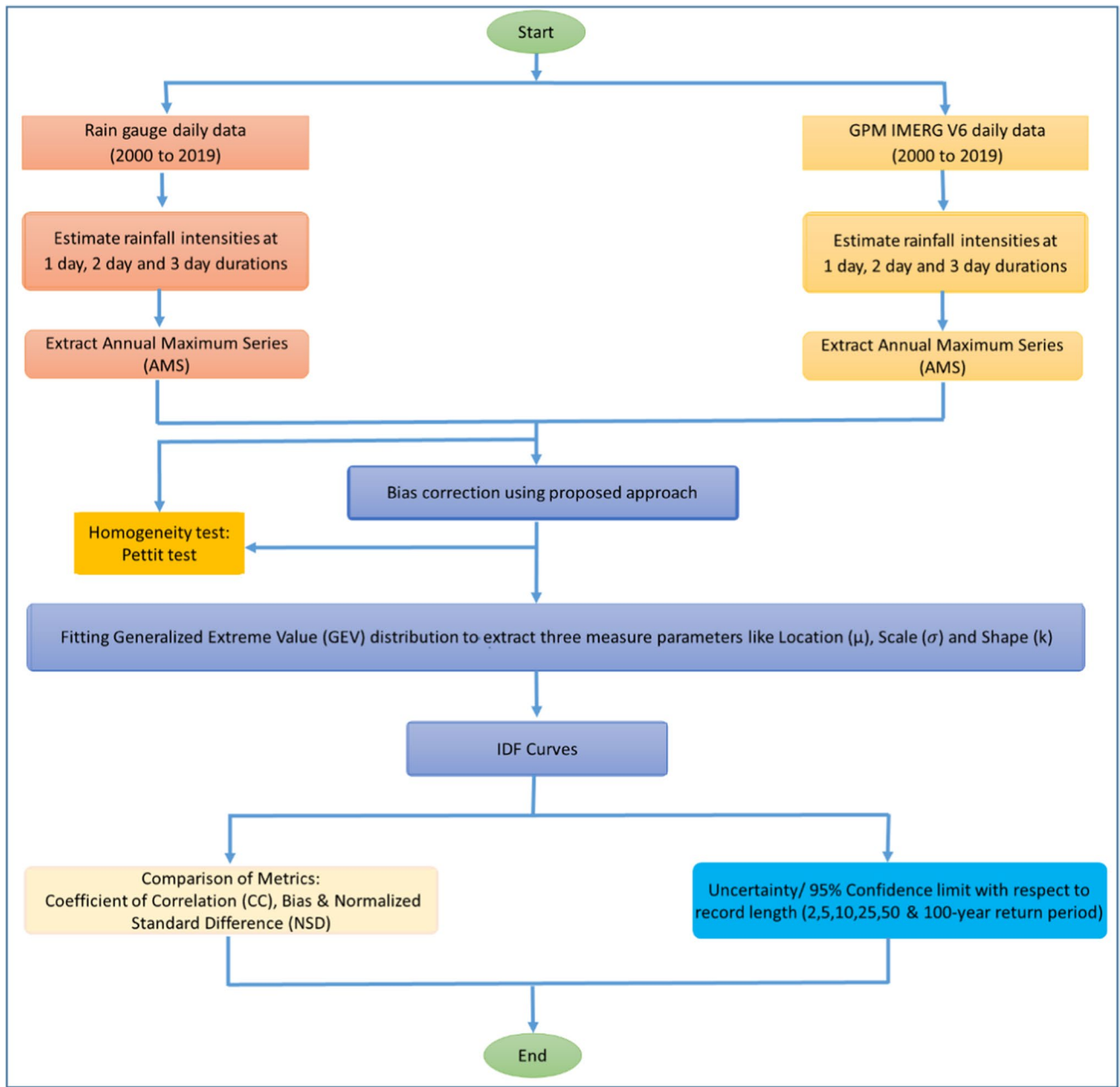


Fig. 2 Flow chart of the proposed methodology

which it detects the change and breakpoints in the time series data and the equation which is given below:

$$U_{(t,n)} = U_{(t-1,n)} + \sum_{(j=1)}^n \text{sgn}(X_t - X_j), 2 \leq t \leq n \tag{1}$$

$$\text{sgn}(X_t - X_j) = \begin{cases} +1 & X_t > X_j \\ 0 & X_t = X_j \\ -1 & X_t < X_j \end{cases} \tag{2}$$

The statistic test counts the no of member of the first sample exceeds the second sample. In the Pettitt test, the null hypothesis is the absence of a change point. The probability (P) and test statistic (K_N) used in the test is given by

$$K_{t_0} = \max_{1 \leq t \leq n} |U_{t,n}| \tag{3}$$

$$P(t_0) \cong 2 \exp \left[-6K_{(t_0)}^2 (n^3 + n^2) \right] \tag{4}$$

when $P(t_0) \leq 0.5$, then there is a significant change point in t_0 .

Biased correction for Satellite-based Precipitation

In recent years, numerous studies have been evaluating the satellite-based precipitation products (Soorooshain et al. 2000; Ebert et al. 2007; Dinku et al. 2008; Behrangi et al. 2011; Duan et al. 2016; Marra et al. 2017; Ozturk et al. 2018, 2021; Marra et al. 2019; Guntu et al. 2020; Setti et al. 2020; Kalyan et al. 2021) and their utilization for different applications. Although these studies vary in many aspects like topography, the time scale of evaluation and valuation metrics, the general agreement is that the satellite precipitation products contain errors, both random and systematic (Zorzzetto et al. 2016; Ombadi et al. 2018; Zorzzetto and Marani 2019). Further, it was also generally observed that some of the products have a lower performance in detecting the heavy rainfall events (Mehran and Aghakouchak 2014; Prakash et al. 2016), thereby necessitating careful examination of errors prior to their application for the development of IDF curves.

For IDF curve generation, only extreme rainfall events, defined as events higher than the 99th percentile of the distribution of total rainfall accumulated over a definite duration of time, are considered. Of the different approaches for sampling the extreme events, the Annual Maximum Series (AMS) is considered in this study as AMS ensures independency of the series's elements and does not require the definition of thresholds (Marra et al. 2017). The error analysis of the GPM data is carried out as given below.

- (i) AMS rainfall values are extracted from the ground measurement data and satellite-based precipitation product (GPM) datasets for all the locations; the length of the AMS series is 19 years extracted for the period from 2001 to 2019.
- (ii) AMS obtained from the gauge and GPM rainfall datasets are given ranks and arranged in descending order.
- (iii) A bias correction factor (ξ) is defined as the ratio of ground measurement to satellite-based precipitation product (GPM) that is,

$$(x, y, l) = \frac{P_{G(x,y,l)}}{P_{S(x,y,l)}} \quad (5)$$

where (x, y, l) is the adjustment factor for the l th event in the AMS at the location (x, y) ,

$P_{G(x,y,l)}$ is the l th ground-based rainfall event in the AMS at the location (x, y) and $P_{S(x,y,l)}$ is the l th Satellite-based rainfall event in the AMS at the location (x, y) .

- (iv) At each grid point location, the average value of the bias for a given location ($\bar{\xi}_{x,y}$) which represents the systematic error in the satellite precipitation product is estimated as

$$\bar{\xi}_{x,y} = \sum_{l=1}^{19} \frac{\xi(x, y, l)}{19} \quad (6)$$

- (v) After estimating the bias in the estimates for each location, the bias-corrected satellite precipitation at a given location (x,y) is estimated by,

$$P_s^{corr}(x,y) = P_{S(x,y)} \times \bar{\xi}_{x,y} \quad (7)$$

For comparison, in this study, IDF curves were developed using both the GPM datasets with and without correction.

Developing intensity duration frequency (IDF) curves

In this study, the Generalized Extreme Value type (GEV) distribution (Appendix A) method is used for developing IDF curves. GEV is a three-parameter extreme value distribution commonly used to model extreme rainfall events (Bougadis and Adamowski 2006; Overeem et al. 2008; Bairwa et al. 2016; Marra et al. 2017; Ombadi et al. 2018). Compared with the other distribution functions like Pearson type III distribution or Generalized logistic distribution, GEV distribution best fits the Annual Maximum Series (AMS) (Kysely and Picek 2007; Perica et al. 2013). Further, GEV distribution has been used for frequency analysis for datasets based on satellites (Overeem et al. 2008; El-dardiry et al. 2015; Paixao et al. 2015; Marra et al. 2016, 2017; Panziera et al. 2016) owing to its ability to include all three (EV-I, EV-II and EV-III) asymptotic extreme values types (Katz et al. 2002).

Based on the reasons mentioned above, in this study, GEV is used to fit the AMS values of maximum rainfall intensities observed over 1-day, 2-day and 3-day durations, obtained from daily gauge data, GPM and biased-corrected GPM precipitation data.

The obtained AMS rainfall intensities values for each point are fitted with GEV distribution, then the IDF Curves are derived for 2, 5, 10, 25, 50 and 100 years return period at 1-day, 2-day and 3-day duration.

Comparison between for derived intensity–duration–frequency maps

In this study, the comparison between the IDF generated using different datasets is performed using the non-dimensional normalized metrics given below. For comparison, the

IDF derived using the observed gauge-based data is used to reference the ones derived from the satellite-based datasets.

Coefficient of Correlation (CC) It computes the spatial correlation between the IDFs generated from the gauge data and the satellite product across different locations at given return periods. The values range between -1 and 1 with +1 indicating that the estimates from both datasets perfectly match the spatial variation of the estimates from both datasets. It can be computed by using Eq. (8)

Bias It measures the mean quantitative agreement of the derived IDF curves. Generally, the bias values should be greater or less than 1. The +1 indicates the exact mean quantity agreement. A lower value indicates that the mean of satellite-based precipitation evaluation is greater than the mean of ground-based gauge estimate. It can be estimated using Eq. (9)

Normalized standard difference (NSD) It measures the standard deviation of the residuals of the normalized values is calculated as Eq. (10) (Marra et al. 2017). NSD values are generally ≥ 0 , with values near to zero are desirable.

Percentage relative error (RE) The percentage relative error is the accepted metric for the absolute values of rainfall estimates. This metric evaluation allows computing the overall performances of derived IDF curves over the entire study region.

$$CC(d, T) = \frac{Cov(\mathbf{G}_{d,T}, \mathbf{S}_{d,T})}{Stdev(\mathbf{G}_{d,T}) \cdot SD(\mathbf{S}_{d,T})} \tag{8}$$

$$Bias(d, T) = \frac{\sum_i^N g_{d,T}^i}{\sum_i^N s_{d,T}^i} \tag{9}$$

$$NSD(d, T) = \sqrt{\frac{1}{N} \sum_i^N \left[\frac{s_{d,T}^i}{\bar{s}_{d,T}} - \frac{g_{d,T}^i}{\bar{g}_{d,T}} \right]^2} \tag{10}$$

$$RE = \left(\frac{IDF_{Satellitebasedprecipitation} - IDF_{Groundbasedgaugeprecipitation}}{IDF_{Groundbasedgaugeprecipitation}} \right) \tag{11}$$

Where $\mathbf{S}_{d,T}$ and $\mathbf{G}_{d,T}$ represents vector (1xN) rainfall intensities estimated from the fitted GEV at d-day duration with T year return period; $g_{d,T}^i$ and $s_{d,T}^i$ are the gauge IDF and satellite IDF estimates at the ith location within the total number of N locations; $\bar{g}_{d,T}$ and $\bar{s}_{d,T}$ are the mean values of the gauge and satellite estimates.

Estimation of confidence intervals

The confidence intervals are estimated using the Monte Carlo bootstrapping method following the method described in Ombadi et al. 2018. The methods consist of three steps.

1. Empirical CDF is estimated from the gauge data at all nine locations using Kernel Density estimation (Rosenbalt 1956; Ombadi et al. 2018).
2. From the empirical distribution, samples with the same length of record (19 years) are extracted. Random samples were drawn from the uniform distribution in the range [0 1], then the corresponding quantiles were estimated from the empirical CDF.
3. The Monte Carlo sampling is done 1000 times to get the asymptotic properties. The 95th and 5th percentiles were estimated to get the 90% confidence interval based on the obtained values.

Results and discussion

Homogeneity tests

Pettitt test is applied to the extreme annual rainfall daily data for each ground-based gauge point precipitation data, GPM precipitation and biased corrected GPM precipitation data. The results obtained using the Pettit test for different precipitation products are shown in Table 2: The k-statistic value and p value are given for a significance level of 0.05 at a 95% confidence interval. Overall, p values from Petit's test show that the data is homogeneous and can be used for the IDF generation.

Bias correction

Figure 3 shows the Q–Q plot between the gauge-based quantiles and the quantiles from satellite data before and after adjustment for one location. Figure 4 demonstrates significant improvement in the quantiles estimated from the GPM after the bias correction. Further, the bias correction removes the significant part of systematic error as seen from the close alignment of the quantiles values towards the X = Y line after bias correction. It can be discerned from Fig. 3 that the bias correction results in improves the estimation of the AMS value. This analysis highlights that bias correction is effective in removing bias in satellite precipitation.

Table 2 The k-statistic value, pvalue and point detected location values are given for a significance level of $\alpha=0.05$ for 9 different location points

Station point	Pettit test					
	K Static			<i>p value</i>		
	Ground based gauge point	GPM	Biased corrected GPM	Ground based gauge point	GPM	Biased corrected GPM
P1	34	33	33	0.765	0.885	0.905
P2	39	39	39	0.554	0.546	0.533
P3	39	43	43	0.54	0.361	0.351
P4	25	41	41	0.465	0.441	0.429
P5	37	79	79	0.645	0.0001	0.001
P6	24	31	31	0.403	0.945	0.95
P7	47	20	20	0.23	0.174	0.164
P8	55	37	37	0.084	0.645	0.65
P9	29	61	61	0.788	0.03	0.032

If the *p value* is less than the significance level α , then we can reject the null hypothesis that the data is homogeneous

If the *p value* is greater than the significance level, then we can accept the null hypothesis

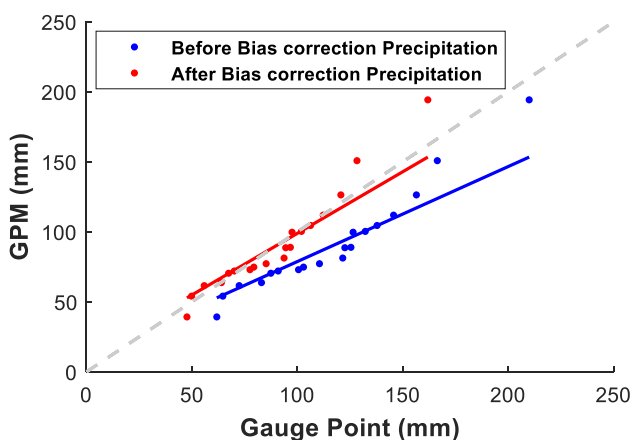


Fig. 3 Q-Q plots comparing quantiles of AMS extracted from the ground-based gauge point, GPM and biased corrected GPM. The red colour represent GPM precipitation, and blue colour represents biased corrected GPM precipitation

Assessment of satellite-based and ground-based GEV parameters

The obtained AMS data from 1-day, 2-day and 3-day from rain guage, GPM and bias-corrected GPM datasets at all the locations are fitted GEV distribution to obtain parameters like location (μ) parameter, scale (σ) parameter and shape (k). The median and the 25–75th quantile intervals of the parameters (over the all the locations) derived from the three datasets are shown in Fig. 4.

The location parameters from the GPM are larger than the ones from the gauges, meaning that the extreme values from the GPM are in general higher than the observed values. Marra et al. 2017 assert that the location parameters'

differences can be associated with the bias in the extreme values and can be removed by suitable bias correction. Figure 4 shows that the location parameters obtained using the bias-corrected GPM are closer to the observed values for all the duration.

For comparison, the scale parameters are normalized by considering the corresponding location parameters. The normalized scale parameters from the GPM dataset tend to derive high scale parameters suggesting higher dispersion. However, increasing the duration, the scale parameters' value tends to decrease for all the three datasets, and the difference in values tends to reduce.

Analysis of the shape parameters obtained shows that mostly $k > 0$ for all the three datasets and durations, suggesting that thick-tailed distribution better describes extreme rainfall events in this area. As evident from the figure, the shape parameters were similar to those obtained using the gauges. The parameters obtained using the bias-corrected GPM were similar in terms of the median, but the variability is slightly higher than the gauge-based estimates. Further, with increased duration, the shape parameters values tend to increase, suggesting more thicker tailed distribution.

Comparison of derived IDF curves

Using the estimated GEV parameters, the IDF curves were derived for different return period, $T = 2, 5, 10, 25, 50, 100$ years at all the locations considered in the study. The intensity of rainfall vs duration for $T = 2$ years and $T = 25$ years is shown in Fig. 5a, b. As evident from Fig. 5a, the derived IDF curves using gauge data and bias-corrected GPM are closer for most locations except for Point 5, where there is an underestimation.

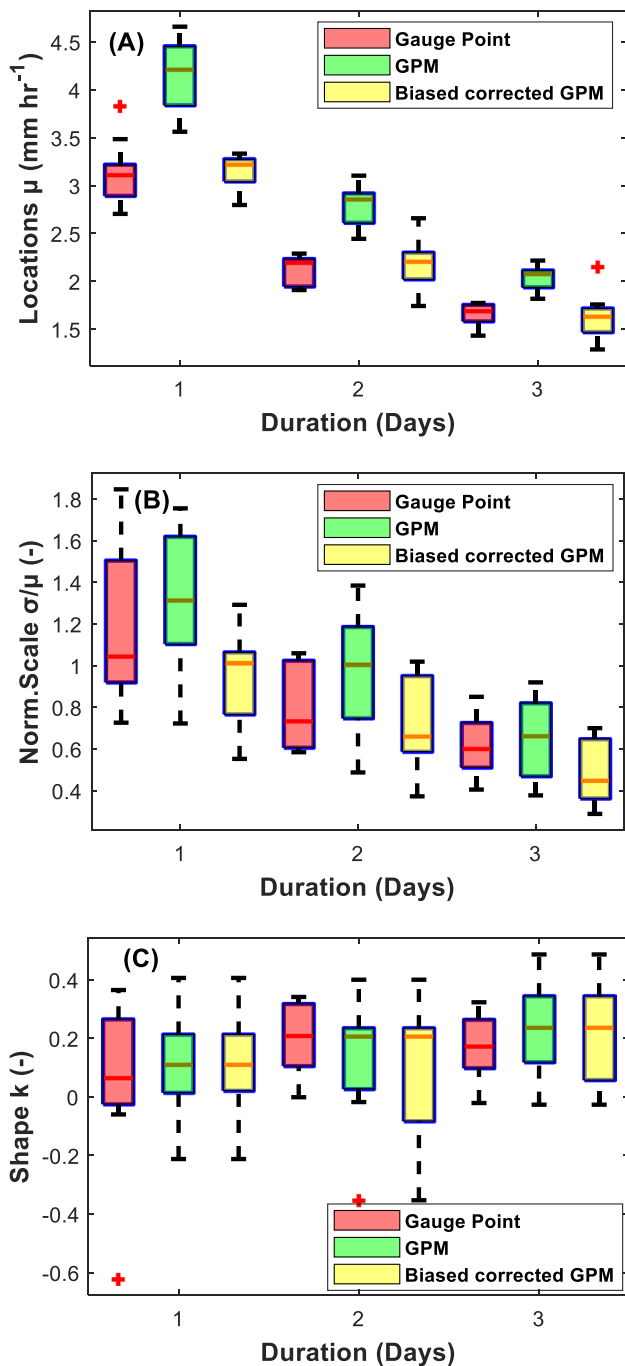


Fig. 4 The variation between the obtained GEV parameters like location (μ), scale (σ) and shape (k) parameters from ground-based gauge point, satellite-based- GPM and Biased-corrected GPM precipitation product over 1 day, 2 day and 3 day duration

However, there is a significant overestimation of the intensity values using the GPM data, which was also evident from the corresponding location parameters.

Comparing the 25-year estimate of the rainfall intensity (as shown in Fig. 5b) obtained using the bias-corrected GPM, there is a tendency to underestimate at most locations

except at points 1 and 4. Interestingly, the estimates at points 5 and 9 based on GPM closely match the gauge-based estimates from bias-corrected GPM. This could be due to an outlier in the AMS values from that location because the overall bias correction value was affected.

Overall, based on the IDF curves' visual comparison, the bias-corrected GPM-based estimates were closer to the gauge-based estimates.

The IDF maps for 1-day duration at three different return periods obtained from the gauge, GPM and bias-corrected GPM are presented in Fig. 6. It can be seen that the IDF values are higher in the southern part of the study, which is closer to the Indian Ocean. The IDF maps based on GPM tend to overestimate the intensities, particularly in the southern part of the study region. Even though there is a significant improvement in the bias-corrected GPM derived IDF maps, there are still pockets of locations in the southern part where there is significant overestimation compared to the gauge-based estimates. The bias-corrected GPM IDF maps are comparable with those from the gauges for a higher return period than for a lower return period ($T=2$ years). A detailed quantitative analysis of the differences between the IDF maps derived from the different datasets is given in the next section.

Comparison of non-dimensional metrics between IDF of ground-based gauge point—GPM and ground-based gauge point—biased corrected GPM

The complete quantitative comparison in terms of non-dimensional metrics like Coefficient of Correlation (CC), Bias and Normalized standard differences (NSD) between the GPM and Biased corrected GPM IDF maps are shown in Fig. 7. A significant difference is observed in the pattern of CC for GPM and bias-corrected GPM. The CC, which measures the spatial correlation of the IDF maps is as high as approximately 0.74–0.8 for 2 years and 5-year return periods and reduces when higher return periods are considered. The bias-corrected GPM exhibits a higher correlation at all return periods and duration than the GPM. Interestingly, the bias correction factor improved the magnitude and also the spatial organization of the annual extremes.

Bias values less than 1 indicates that the GPM tends to overestimate the rainfall intensities, whereas the bias values were closer for bias-corrected GPM, meaning that the bias correction improves the results significantly. Noteworthy, the bias values were of the same magnitude for all the return periods and durations. Similar behavior was observed by (Marra et al. 2017) wherein the authors report the bias is the same for return periods at higher durations.

The difference in NSD tends to decrease with the return period and the duration. The bias-corrected GPM tends

Fig. 5 a Comparison of 2-year return period for 1-day, 2-day and 3-day duration for ground-based gauge point, GPM and Biased-corrected GPM for 9 grid point data and **b** Comparison of 25-year return period for rain gauge GPM and Biased-corrected GPM for nine grid-point data

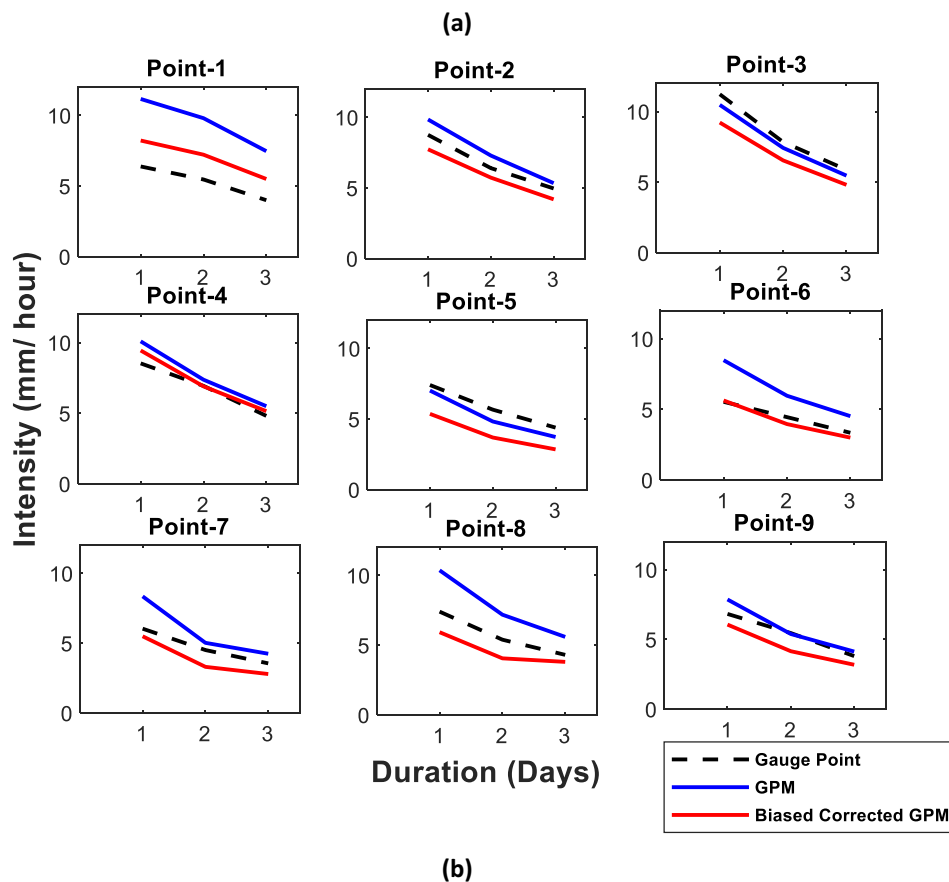
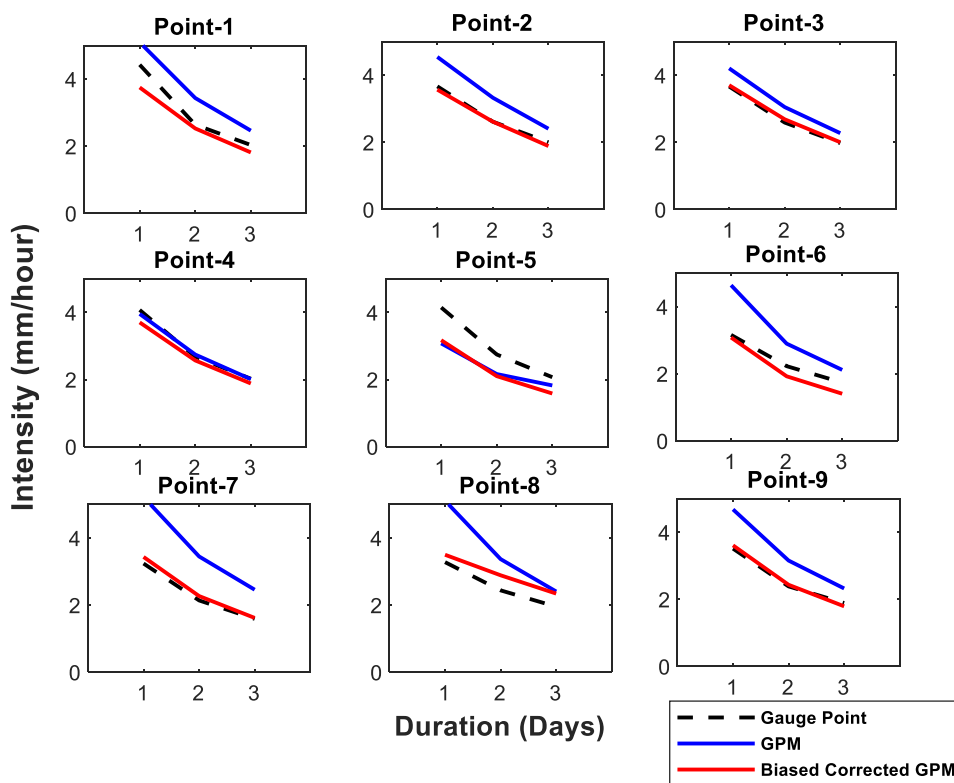


Fig. 6 Comparison of Spatially distribution/Interpolated maps for 2-year, 10 year, and 25 year return periods of Ground-based gauge precipitation, GPM and Biased-corrected GPM precipitation data

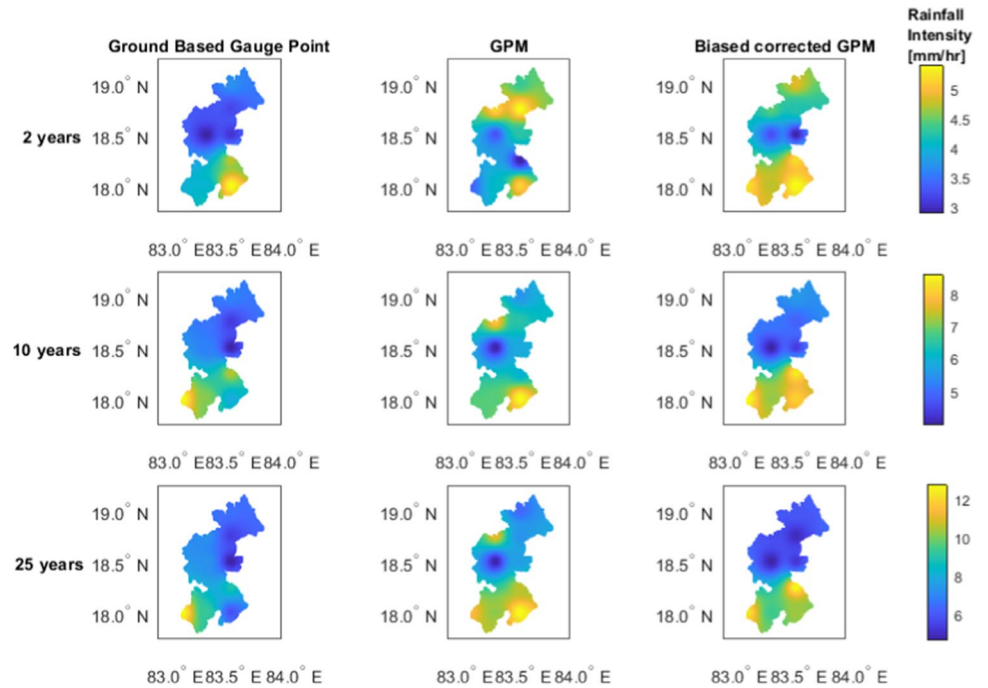
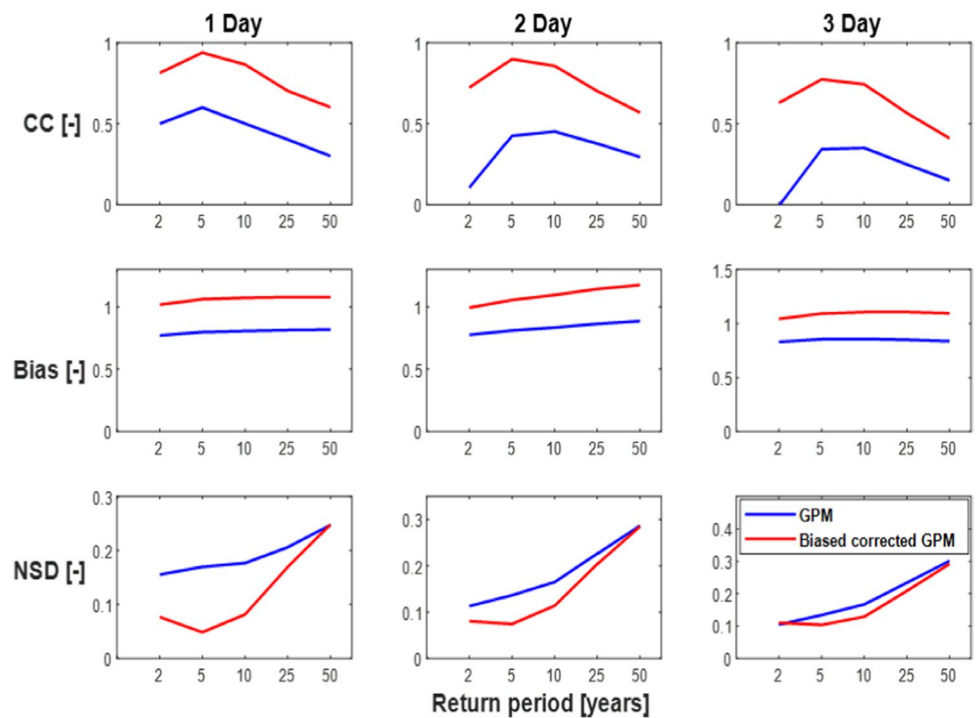


Fig. 7 Comparison of non-dimensional metric parameters of Coefficient of correlation (cc), Bias and NSD for 1-Day, 2-Day and 3-Day duration. The first row represents the CC, the middle row represents the bias, and the last row represents the NSD for 1-Day, 2-Day and 3-Day durations



to have lesser NSD at lower return periods but has similar NSD (to GPM) at larger return periods. A similar trend was observed at longer durations, but the gap between the two was reduced with the increase in duration. According to Mei et al. (2016) results shows that the regularly monitored gauge data impacts the annual extreme rainfall events when compared with the satellite-based obtained annual extreme rainfall events.

The percentage relative error for the remotely sensed precipitation data, i.e., GPM and biased corrected GPM precipitation data, are shown in Fig. 8. It can be seen that the biased corrected GPM product performs well in providing the least percentage relative error. The GPM dataset without bias possesses a percentage relative error vary from 5 to 40%, whereas, in the biased corrected GPM precipitation product, it is comparatively less for all return periods. Across

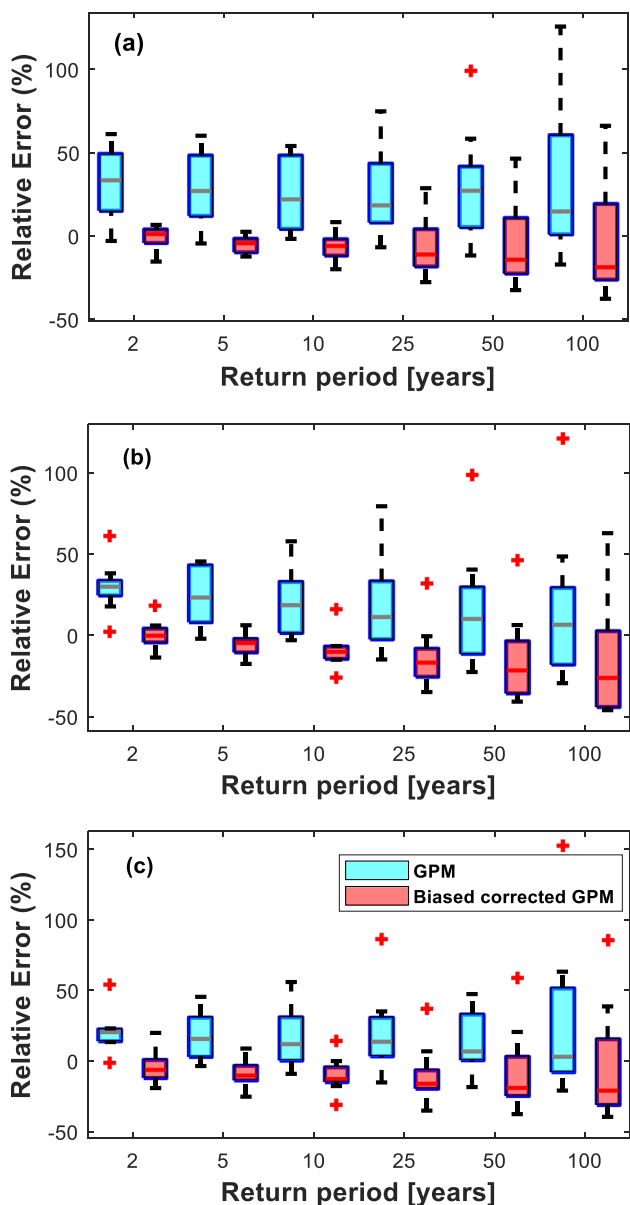


Fig. 8 Relative error present in ground-based gauge point -GPM and ground-based gauge point—biased corrected GPM IDF return period values are represented in the form of boxplot for **a** 1 day. **b** 2 day. **c** 3 day. The light blue thick line present in the box represents the median value and the boxes represent the interquartile range, and the thick dashed lines represent the range

the different durations, the error range is reducing with the increased duration, indicating that aggregating the rainfall values reduces the difference in the precipitation products. On the other hand the range of the error is increasing with the return period as expected.

Figure 9 reports the IDF curves obtained from the different datasets at all locations and the confidence interval estimated using the method elaborated in Sect. 3.5. The IDF curves.

The estimates obtained using the different datasets are within the confidence interval for durations. However, the quantiles obtained using the GPM were overestimated compared to ones obtained from the gauge data at P1, P2, P4, P7, P7, P8, and underestimated at P3, P5. There is a significant improvement in the IDF curve estimates using the bias-corrected wherein the IDF curves are closer to the gauge-based IDF. A similar pattern was observed across the different durations.

Interestingly, the estimates from GPM data without bias correction were closer to gauge IDF at P2, P3, and P5 locations. The bias correction exaggerates the error, leading to increased underestimation at these locations. This emphasizes that while the bias correction is essential for developing accurate IDF curves, special attention must be given to regions where the satellite products show a different behavior, such as the case over the eastern part (P2, P3 and P5) of the study region.

This study reveals the applicability of satellite-based products for deriving the IDF curves. However, there are different levels of uncertainty (retrieval stage, downscaling, bias correction methods, extreme event selection method, parameter estimation) that arise in the estimation of IDF curves and the quantification of the same can be considered as a future study.

Conclusion

This work aims to investigate the application of the satellite precipitation products in deriving IDF curves, particularly in developing countries where the rain gauge network is sparse and has lesser spatial coverage/record length. With the advancement in space technology and retrieval method of precipitation from satellites, it is important to assess these precipitation products accurately. This study has attempted in assessing recent GPM products and a methodology to derive IDF curves from the satellite products.

With this motivation, the application of GPM-IMERG-V6 for IDF generation in the developing countries, we have considered a small region in the southern part of India where ground gauge area available insufficient length.

The shape parameters of the GEV distribution as derived from the satellite precipitation and gauge are greater than “zero”. The location parameters from the satellite precipitation (GPM) are larger than those from the gauges, meaning that the extreme values from the (GPM) are generally higher than the observed values. The normalized scale parameters from the GPM dataset tend to derive high scale parameters suggesting higher dispersion. However, increasing the duration, the scale parameters’ value tends to decrease for all the three datasets, and the difference in values tends to reduce. The percentage relative error median values of GPM return

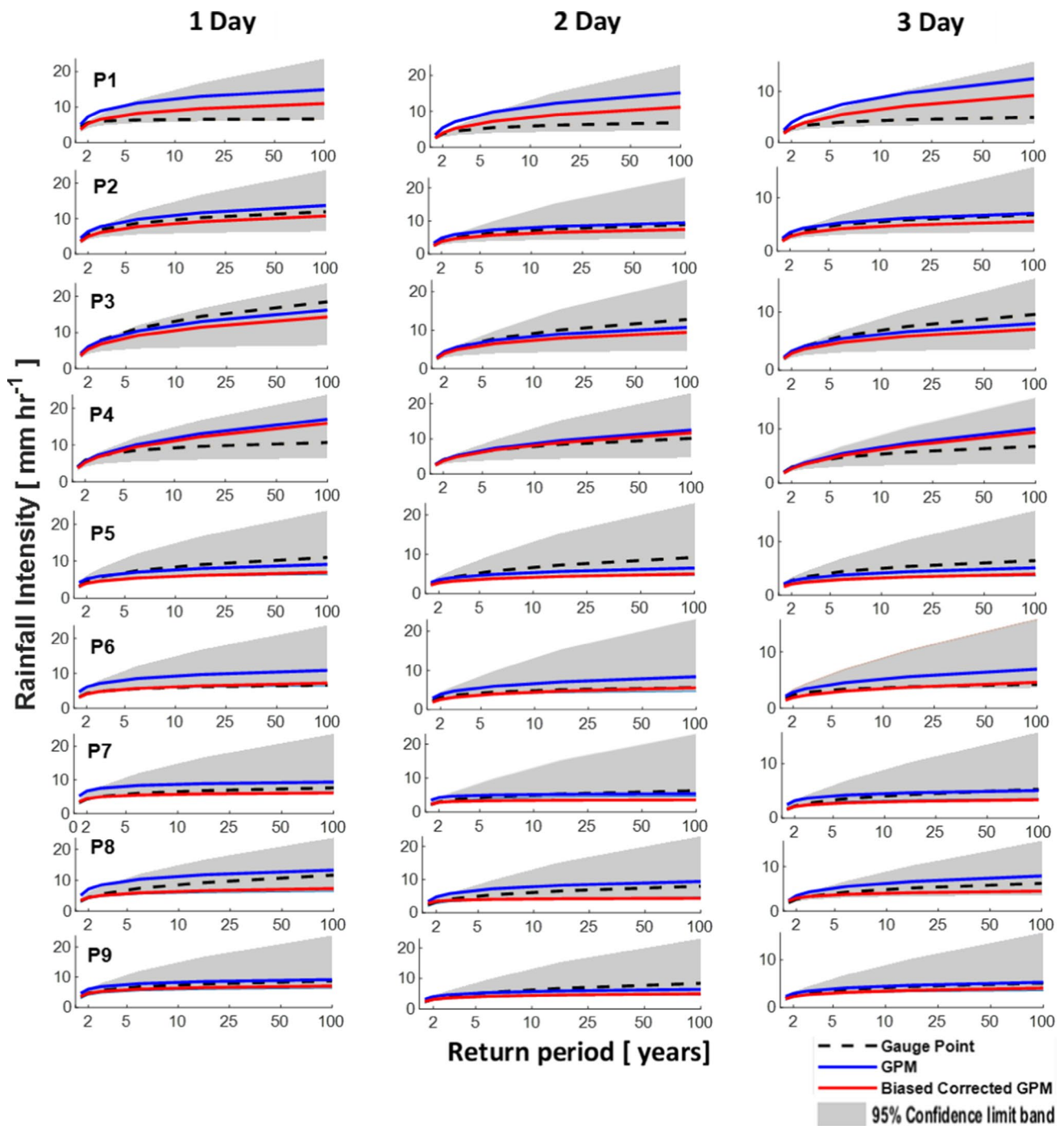


Fig. 9 Visual Comparison of IDF curves for 2-year, 5-year, 10-year, 25- year, 50-year and 100-year return period values for satellite-based precipitation GPM (red line) and bias corrected GPM data

over ground-based gauge (dashed black line) data at nine location for 1-day, 2-day and 3 day durations. The 95% confidence interval band is represented in the shaded area (grey)

periods vary from 5 to 40%, whereas, in the Biased corrected GPM precipitation product, the percentage relative error values are less than 15%. The estimates from the bias-corrected product are robust for most of the study region,

but at two locations, the model has limitations in adjusting the underestimation.

Even though the present study focused on a small region, the methodology can be extended to large river basins /regions. Overall, the study results emphasize the

potential use of the GPM satellite precipitation as an alternative data for developing IDF curves in developing countries. There are several future works emanate from this study. These include quantifying the different sources of uncertainty that arise at various levels, such as estimation algorithms, bias correction methods, parameter estimation methods, etc.

Appendix A

The Generalized Extreme Value (GEV) type distribution method is defined below equation:

(i) For $k \neq 0$:

$$F = (I; \mu; \sigma; k) = \exp \left\{ - \left[1 + \frac{k}{\sigma} (1 - \mu) \right]^{-1/k} \right\} \quad (12)$$

(ii) For $k = 0$:

$$F = (I; \mu; \sigma; k) = \exp \left\{ - \exp \left[- \frac{1}{\sigma} (1 - \mu) \right] \right\} \quad (13)$$

Where: 'I' is the rainfall intensities derived for 1-day, 2-day, 3-day duration. The location (μ), scale (σ) and shape (k) are the GEV distribution parameters. The tail of the extreme values distribution is direct with the shape parameter (k). The shape parameter (k) of low (high) is related to lower (higher), which are having a more significant extreme probability. We use the Type III distribution method. When shape (k) is zero, then we can expect extreme values at the upper limit. We adopted Type II or equal Type I distribution when shape parameter (k) is 0 then. In this case, we cannot expect an upper limit. If the k is greater than 0.5 and 1, then the mean and standard deviation of the distribution tends to ' ∞ '. According to the Fisher-Tippet theorem validates that Generalized Extreme Value Type Distribution is one of the most probable distribution functions for similar distributed random variables of extreme values.

Acknowledgements Dr.R.Maheswaran gratefully acknowledges the funding received from the Department of Science and Technology, Water Technology Initiative under the project DST/WTI/DD/2k17/0079.

References

- Agarwal A, Marwan N, Rathinasamy M, Merz B, Kurths J (2017) Multi-scale event synchronization analysis for unravelling climate processes: a wavelet-based approach. *Nonlinear Process Geophys* 24:599–611. <https://doi.org/10.5194/npg-24-599-2017>
- Agarwal A, Maheswaran R, Marwan N, Caesar L, Kurths J (2018) Wavelet-based multiscale similarity measure for complex networks. *Eur Phys J B* 91(11):1–12. <https://doi.org/10.1140/epjb/e2018-90460-6>
- Agarwal A, Caesar L, Marwan N, Maheswaran R, Merz B, Kurths (2019) Network-based identification and characterization of teleconnections on different scales. *Sci Rep* 9:1–12. <https://doi.org/10.1038/s41598-019-45423-5>
- Agarwal A, Marwan N, Maheswaran R, Merz B, Kurths J (2020) Optimal design of hydrometric station networks based on complex network analysis. *Hydrol Earth Syst Sci* 24:2235–2251. <https://doi.org/10.5194/hess-24-2235-2020>
- Aghakouchak A, Behrangi A, Sorooshian S, Hsu K, Amitai E (2011) Evaluation of satellite-retrieved extreme precipitation rates across the central United States. *J Geophys Res Atmos* 116:1–11. <https://doi.org/10.1029/2010JD014741>
- Ahmed E, Al Janabi F, Zhang J, Yang W, Saddique N, Kerbs P (2020) Hydrologic assessment of TRMM and GPM-based precipitation products in transboundary river catchment (Chenab River, Pakistan). *Water* 12:1–20. <https://doi.org/10.3390/w12071902>
- AlHassoun SA (2011) Developing an empirical formulae to estimate rainfall intensity in Riyadh region. *J King Saud Univ - Eng Sci* 23:81–88. <https://doi.org/10.1016/j.jksues.2011.03.003>
- Amitai E, Petersen W, Lloret X, Vasiloff S (2012) Multiplatform comparisons of rain intensity for extreme precipitation events. *IEEE Trans Geosci Remote Sens* 50:675–686. <https://doi.org/10.1109/TGRS.2011.2162737>
- Awadallah AG, ElGamal M, ElMostafa A, ElBadry H (2011) Developing intensity-duration-frequency curves in scarce data region: an approach using regional analysis and satellite data. *Engineering* 03:215–226. <https://doi.org/10.4236/eng.2011.33025>
- Bairwa AK, Khosa R, Maheswaran R (2016) Developing intensity duration frequency curves based on scaling theory using linear probability weighted moments: a case study from India. *J Hydrol* 542:850–859. <https://doi.org/10.1016/j.jhydrol.2016.09.056>
- Behrangi A, Khakbaz B, Jaw TC, AghaKouchak A, Hsu K, Sorooshian S (2011) Hydrologic evaluation of satellite precipitation products over a mid-size basin. *J Hydrol* 397:225–237. <https://doi.org/10.1016/j.jhydrol.2010.11.043>
- Bhatt S, Ahmed SA (2014) Morphometric analysis to determine floods in the Upper Krishna basin using Cartosat DEM. *Geocarto Int* 29:878–894. <https://doi.org/10.1080/10106049.2013.868042>
- Bougadis J, Adamowski K (2006) Scaling model of a rainfall intensity-duration-frequency relationship. *Hydrol Process* 20:3747–3757. <https://doi.org/10.1002/hyp.6386>
- Chen S, Hong Yang H, Qing C, Pierre EK, Jonathan JG, Youcun Q, Jian Z, Howard K, Junjun H, Jun W (2013) Performance evaluation of radar and satellite rainfalls for Typhoon Morakot over Taiwan: are remote-sensing products ready for gauge denial scenario of extreme events? *J Hydrol* 506:4–13. <https://doi.org/10.1016/j.jhydrol.2012.12.026>
- Chen C, Chen Q, Duan Z, Zhang J, Mo K, Li Z, Tang G (2018) Multi-scale comparative evaluation of the GPM IMERG v5 and TRMM 3B42 v7 precipitation products from 2015 to 2017 over a climate transition area of China. *Remote Sens* 10:1–18. <https://doi.org/10.3390/rs10060944>
- Cheng L, AghaKouchak A, Gilleland E, Katz RW (2014) Non-stationary extreme value analysis in a changing climate. *Clim Change* 127:353–369. <https://doi.org/10.1007/s10584-014-1254-5>
- Chow VT, Maidment DR, Mays LW (1988) *Applied hydrology*. McGraw-Hill, New York, p 572p
- Costa AC, Soares A (2009) Homogenization of climate data: review and new perspectives using geostatistics. *Math Geosci* 41:291–305. <https://doi.org/10.1007/s11004-008-9203-3>
- Cross R (2010) World disasters report (2010) focus on urban risk. International Federation of Red Cross and Red Crescent Societies, Geneva

- Dash SS, Kumar HH (2017) Statistical and trend analysis of climate data of bapatla(AP). *India Int J Curr Microbial Appl Sci* 6:4959–4969
- Dinku T, Chidzambwa S, Ceccato P, Connor SJ, Ropelewski CF (2008) Validation of high-resolution satellite rainfall products over complex terrain. *Int J Remote Sens* 29:4097–4110. <https://doi.org/10.1080/01431160701772526>
- Dong P, Wang C, Ding J (2013) Estimating glacier volume loss using remotely sensed images, digital elevation data, and GIS modeling. *Int J Remote Sens* 34:8881–8892. <https://doi.org/10.1080/01431161.2013.853893>
- Duan Z, Liu J, Tuo Y, Chiogna G, Disse M (2016) Evaluation of eight high spatial resolution gridded precipitation products in adige basin (Italy) at multiple temporal and spatial scales. *Sci Total Environ* 573:1536–1553. <https://doi.org/10.1016/j.scitotenv.2016.08.213>
- Ebert EE, Janowiak JE, Kidd C (2007) Comparison of near-real-time precipitation estimates from satellite observations and numerical models. *Bull Am Meteorol Soc* 88:47–64. <https://doi.org/10.1175/BAMS-88-1-47>
- Eldardiry H, Habib E, Zhang Y (2015) On the use of radar-based quantitative precipitation estimates for precipitation frequency analysis. *J Hydrol* 531:441–453. <https://doi.org/10.1016/j.jhydrol.2015.05.016>
- Endreny TA, Imbeah N (2009) Generating robust rainfall intensity-duration-frequency estimates with short-record satellite data. *J Hydrol* 371:182–191. <https://doi.org/10.1016/j.jhydrol.2009.03.027>
- Gado TA, Hsu K, Sorooshian S (2017) Rainfall frequency analysis for ungauged sites using satellite precipitation products. *J Hydrol* 554:646–655. <https://doi.org/10.1016/j.jhydrol.2017.09.043>
- García-Marín AP, Estévez J, Morbidelli R, Saltalippi C, Ayuso-Munoz JL, Flammini A (2020) Assessing inhomogeneities in extreme annual rainfall data series by multifractal approach. *Water* 12:1–18. <https://doi.org/10.3390/W12041030>
- Greco M, Olson WS, Munchak SJ et al (2016) The GPM combined algorithm. *J Atmos Ocean Technol* 33:2225–2245. <https://doi.org/10.1175/JTECH-D-16-00019.1>
- Greenwood JA, Landwehr JM, Matalas NC, Wallis JR (1979) Probability weighted moments: definition and relation to parameters of several distributions expressible in inverse form. *Water Resour Res* 15:1049–1054. <https://doi.org/10.1029/WR015i005p01049>
- Guntu RK, Rathinasamy M, Agarwal A, Sivakumar B (2020) Spatiotemporal variability of Indian rainfall using multiscale entropy. *J Hydrol* 587:124916. <https://doi.org/10.1016/j.jhydrol.2020.124916>
- Hisham Abd El-Kareem El-Dardiry (2014) The use of multi-sensor quantitative precipitation estimates for deriving extreme precipitation frequencies with application in Louisiana
- Hosking JRM, Wallis JR (1993) Some statistics useful in regional frequency analysis. *Water Resour Res* 29:271–281. <https://doi.org/10.1029/92WR01980>
- Huffman G, Bolvin DT, Braithwaite D, Hsu K, Joyce R, Xie P, Yoo SH (2013) Algorithm theoretical basis document (ATBD) NASA global precipitation measurement (GPM) integrated multi-satellite retrievals for GPM (IMERG). Nasa 29
- Huffman G, Bolvin D, Braithwaite D, et al (2015) Algorithm Theoretical Basis Document (ATBD) NASA Global Precipitation Measurement (GPM) Integrated Multi-satellite Retrievals for GPM (IMERG). Nasa 29
- Hurtado SI, Zaninelli PG, Agosta EA (2020) A multi-breakpoint methodology to detect changes in climatic time series. An application to wet season precipitation in subtropical Argentina. *Atmos Res* 241:104955. <https://doi.org/10.1016/j.atmosres.2020.104955>
- Kalyan AVS, Ghose DK, Thalagapu R, Guntu RK, Agarwal A, Kurths J, Rathinasamy M (2021) Multiscale spatiotemporal analysis of extreme events in the Gomati River Basin, India. *Atmosphere (basel)* 12:1–23. <https://doi.org/10.3390/atmos12040480>
- Kasi V, Pinninti R, Landa SR, Rathinasamy M, Sangamreddi C, Kuppili RR, Radha PRD (2020a) Comparison of different digital elevation models for drainage morphometric parameters: a case study from South India. *Arab J Geosci* 13:1–17. <https://doi.org/10.1007/s12517-020-06049-4>
- Kasi V, Yeditha PK, Rathinasamy M, Pinninti R, Landa SR, Sangamreddi C, Agarwal A, Radha PRD (2020b) A novel method to improve vertical accuracy of CARTOSAT DEM using machine learning models. *Earth Sci Informatics* 13:1139–1150. <https://doi.org/10.1007/s12145-020-00494-1>
- Katz RW, Parlange MB, Naveau P (2002) Statistics of extremes in hydrology. *Adv Water Resour* 25:1287–1304. [https://doi.org/10.1016/S0309-1708\(02\)00056-8](https://doi.org/10.1016/S0309-1708(02)00056-8)
- Khan S, Maggioni V (2019) Assessment of level-3 gridded global precipitation mission (GPM) products over oceans. *Remote Sens.* <https://doi.org/10.3390/rs11030255>
- Kisi O (2015) An innovative method for trend analysis of monthly pan evaporations. *J Hydrol* 527:1123–1129. <https://doi.org/10.1016/j.jhydrol.2015.06.009>
- Koutsoyiannis D, Kozonis D, Manetas A, (1998) Intensity-duration-frequency relationships 206, 118–135
- Kumar YP, Maheswaran R, Agarwal A, Sivakumar B (2021) Inter-comparison of downscaling methods for daily precipitation with emphasis on wavelet-based hybrid models. *J Hydrol* 599:126373. <https://doi.org/10.1016/j.jhydrol.2021.126373>
- Kysely J, Picek J (2007) Regional growth curves and improved design value estimates of extreme precipitation events in the Czech Republic. *Clim Res* 33:243–255. <https://doi.org/10.3354/cr033243>
- Le MH, Lakshmi V, Bolten J, Du BD (2020) Adequacy of satellite-derived precipitation estimate for hydrological modeling in Vietnam Basins. *J Hydrol* 586:124820. <https://doi.org/10.1016/j.jhydrol.2020.124820>
- Maheswaran R, Khosa R (2012) Comparative study of different wavelets for hydrologic forecasting. *Comput Geosci* 46:284–295. <https://doi.org/10.1016/j.cageo.2011.12.015>
- Maheswaran R, Khosa R (2013) Wavelets-based non-linear model for real-time daily flow forecasting in Krishna River. *J Hydroinform* 15:1022–1041. <https://doi.org/10.2166/hydro.2013.135>
- Marra F, Nikolopoulos EI, Creutin JD, Borga M (2016) Space–time organization of debris flows-triggering rainfall and its effect on the identification of the rainfall threshold relationship. *J Hydrol* 541:246–255. <https://doi.org/10.1016/j.jhydrol.2015.10.010>
- Marra F, Morin E, Peleg N, Mei Y, Anagnostou EN (2017) Intensity-duration-frequency curves from remote sensing rainfall estimates: comparing satellite and weather radar over the eastern Mediterranean. *Hydrol Earth Syst Sci* 21:2389–2404. <https://doi.org/10.5194/hess-21-2389-2017>
- Marra F, Nikolopoulos EI, Anagnostou EN, Bardossy A, Morin E (2019) Precipitation frequency analysis from remotely sensed datasets: a focused review. *J Hydrol* 574:699–705. <https://doi.org/10.1016/j.jhydrol.2019.04.081>
- Mehran A, Aghakouchak A (2014) Capabilities of satellite precipitation datasets to estimate heavy precipitation rates at different temporal accumulations. *Hydrol Process* 28:2262–2270. <https://doi.org/10.1002/hyp.9779>
- Mei Y, Nikolopoulos EI, Anagnostou EN, Zoccatelli D, Borga M (2016) Error analysis of satellite precipitation-driven modeling of flood events in complex alpine terrain. *Remote Sens* 8(4):293. <https://doi.org/10.3390/rs8040293>
- Naud CM, Booth JF, Lebsack M, Greco M (2018) Observational constraint for precipitation in extratropical cyclones: sensitivity to

- data sources. *J Appl Meteor Climatol* 57:991–1009. <https://doi.org/10.1175/JAMC-D-17-0289.1>
- Ning S, Wang J, Jin J, Ishidaira H (2016) Assessment of the latest gpm-era high-resolution satellite precipitation products by comparison with observation gauge data over the Chinese Mainland. *Water*. <https://doi.org/10.3390/w8110481>
- Noor M, Ismail T, Shahid S, Asaduzzaman M, Dewan A (2021) Evaluating intensity-duration-frequency (IDF) curves of satellite-based precipitation datasets in Peninsular Malaysia. *Atmos Res* 248:105203. <https://doi.org/10.1016/j.atmosres.2020.105203>
- Ombadi M, Nguyen P, Sorooshian S, Hsu K, Lin (2018) Developing intensity-duration-frequency (IDF) curves from satellite-based precipitation: methodology and evaluation. *Water Resour Res* 54:7752–7766. <https://doi.org/10.1029/2018WR022929>
- Omrani E, Sharif HO (2018) Evaluation of the global precipitation measurement (GPM) satellite rainfall products over the lower Colorado River Basin, Texas. *J Am Water Resour Assoc* 54:882–898. <https://doi.org/10.1111/1752-1688.12610>
- Overeem A, Buishand A, Holleman I (2008) Rainfall depth-duration-frequency curves and their uncertainties. *J Hydrol* 348:124–134. <https://doi.org/10.1016/j.jhydrol.2007.09.044>
- Ozturk U, Marwan N, Korup O, Saito H, Agarwal A, Grossman MJ, Zaiki M, Kurths J (2018) Complex networks for tracking extreme rainfall during typhoons. *Chaos*. <https://doi.org/10.1063/1.5004480>
- Ozturk U, Saito H, Matsushi Y, Crisolago I, Schwanghart, (2021) Can global rainfall estimates (satellite and reanalysis) aid landslide hindcasting? *Landslides*. <https://doi.org/10.1007/s10346-021-01689-3>
- Paixao E, Mirza MMQ, Shephard MW, Auld H, Klaassen J, Smith G (2015) An integrated approach for identifying homogeneous regions of extreme rainfall events and estimating IDF curves in Southern Ontario, Canada: Incorporating radar observations. *J Hydrol* 528:734–750. <https://doi.org/10.1016/j.jhydrol.2015.06.015>
- Panziera L, Gabella M, Zanini S, Hering A, Germann U, Berne A (2016) A radar-based regional extreme rainfall analysis to derive the thresholds for a novel automatic alert system in Switzerland. *Hydrol Earth Syst Sci* 20:2317–2332. <https://doi.org/10.5194/hess-20-2317-2016>
- Perica S, Martin D, Pavlovic S, Roy I, Laurent M, Trypaluk C, Unruh D, Yekta M, Bonnin G (2013) Precipitation-frequency atlas of the United States (NOAA Atlas 14, Vol. 8, version 2.0). US Dep Commer, Natl Ocean Atmos Adm Natl Weather Serv Silver Spring, Md 18. <http://www.nws.noaa.gov/oh/hdsc/currentpf.htm>
- Pettitt (1979) A nonparametric to the approach problem. *Appl Stat* 28:126–135
- Pinninti R, Kasi V, Landa SR, Rathinaswamy M, Sangamreddi C, Radha PRD (2021) Investigating the working efficiency of natural wastewater treatment systems: a step towards sustainable systems. *Water Pract Technol*. <https://doi.org/10.2166/wpt.2021.049>
- Prakash S, Mitra AK, Pai DS, AghaKouchak A (2016) From TRMM to GPM: how well can heavy rainfall be detected from space? *Adv Water Resour* 88:1–7. <https://doi.org/10.1016/j.advwatres.2015.11.008>
- Raj S, Shukla R, Trigo RM, Merz B, Rathinasamy M, Ramos AM, Agarwal A (2021) Ranking and characterization of precipitation extremes for the past 113 years for Indian western Himalayas. *Int J Climatol*. <https://doi.org/10.1002/joc.7215>
- Rosenblatt M (1956) Remarks on some nonparametric estimates of a density function. *Ann Mathem Statist*
- Setti S, Rathinasamy M, Chandramouli S (2018) Assessment of water balance for a forest dominated coastal river basin in India using a semi distributed hydrological model. *Model Earth Syst Environ* 4:127–140. <https://doi.org/10.1007/s40808-017-0402-0>
- Setti S, Maheswaran R, Radha D, Sridhar V, Barik KK, Narasimham ML (2020) Attribution of hydrologic changes in a tropical river basin to rainfall variability and land-use change: case study from India. *J Hydrol Eng* 25:1–15. [https://doi.org/10.1061/\(ASCE\)3390/rs9070720](https://doi.org/10.1061/(ASCE)3390/rs9070720)
- Sorooshian S, Hsu KL, Gao X, Gupta HV, Imam B, Braithwaite D (2000) Evaluation of PERSIANN system satellite-based estimates of tropical rainfall. *Bull Am Meteorol Soc* 81:2035–2046. [https://doi.org/10.1175/1520-0477\(2000\)081%3c2035:EOPSSE%3e2.3.CO;2](https://doi.org/10.1175/1520-0477(2000)081%3c2035:EOPSSE%3e2.3.CO;2)
- Stewart EJ, Reed DW, Faulkner DS, Reynard NS (1999) The FORGEX method of rainfall growth estimation I: Review of requirement. *Hydrol Earth Sys Sci* 3:187–95
- Tan ML, Duan Z (2017) Assessment of GPM and TRMM precipitation products over Singapore. *Remote Sens* 9:1–16. <https://doi.org/10.3390/rs9070720>
- Tan J, Huffman GJ, Bolvin DT, Nelkin EJ (2019) IMERG V06: Changes to the morphing algorithm. *J Atmos Ocean Technol* 36:2471–2482. <https://doi.org/10.1175/JTECH-D-19-0114.1>
- Tang G, Zeng Z, Long D, Guo X, Yong B, Zhnag W, Hong Y (2016) Statistical and hydrological comparisons between TRMM and GPM Level-3 products over a midlatitude Basin: Is day-1 IMERG a good successor for TMPA 3B42V7? *J Hydrometeorol* 17:121–137. <https://doi.org/10.1175/JHM-D-15-0059.1>
- Tang G, Clark MP, Papalexioiu SM, Ma Z, Hong Y (2020) Have satellite precipitation products improved over last two decades? A comprehensive comparison of GPM IMERG with nine satellite and reanalysis datasets. *Remote Sens Environ* 240:111697. <https://doi.org/10.1016/j.rse.2020.111697>
- Tapiador FJ, Turk FJ, Petersen W, Hou AY, Garcia-Ortega E, Machado LA, Angelis CF, Salio P, Kidd C, Huffman GJ, De Castro M (2012) Global precipitation measurement: methods, datasets and applications. *Atmos Res* 104–105:70–97. <https://doi.org/10.1016/j.atmosres.2011.10.021>
- Tfwala CM, van Rensburg LD, Schall R, Mosia SM, Dlamini P (2017) Precipitation intensity-duration-frequency curves and their uncertainties for Ghaap plateau. *Clim Risk Manag* 16:1–9. <https://doi.org/10.1016/j.crm.2017.04.004>
- Vivekanandan N (2013) Analysis of hourly rainfall data for the development of IDF relationships using the order statistics approach of probability distributions. *Int J Manag Sci Eng Manag* 8:283–291. <https://doi.org/10.1080/17509653.2013.829630>
- Wang X, Ding Y, Zhao C, Wang J (2019) Similarities and improvements of GPM IMERG upon TRMM 3B42 precipitation product under complex topographic and climatic conditions over Hexi region, Northeastern Tibetan Plateau. *Atmos Res* 218:347–363. <https://doi.org/10.1016/j.atmosres.2018.12.011>
- Watt E, Marsalek J (2013) Critical review of the evolution of the design storm event concept. *Can J Civ Eng* 40:105–113. <https://doi.org/10.1139/cjce-2011-0594>
- Wayal AS, Menon K (2014) Intensity–duration–frequency curves and regionalization. *Int J Innov Res Adv Eng* 1:28–32
- Wijngaard JB, Klein Tank AMG, Können GP (2003) Homogeneity of 20th century European daily temperature and precipitation series. *Int J Climatol* 23:679–692. <https://doi.org/10.1002/joc.906>
- World Development Report, World Development Report (2018) Learning to Realize Education’s Promise (The World Bank, 2018)
- Yang H, Qi J, Xu X, Yang D, Lv H (2014) The regional variation in climate elasticity and climate contribution to runoff across China. *J Hydrol* 517:607–616. <https://doi.org/10.1016/j.jhydrol.2014.05.062>
- Yeditha PK, Kasi V, Rathinasamy M, Agarwal A (2020) Forecasting of extreme flood events using different satellite precipitation products and wavelet-based machine learning methods. *Chaos* 30:063115. <https://doi.org/10.1063/5.0008195>
- Yong B, Liu D, Gourley JJ, Tian Y, Huffman GJ, Ren L, Hong Y (2015) Global view of real-time TRMM multisatellite precipitation

- analysis: Implications for its successor global precipitation measurement mission. *Bull Am Meteorol Soc* 96:283–296. <https://doi.org/10.1175/BAMS-D-14-00017.1>
- Zhang S, Wang D, Qin Z et al (2018) Assessment of the GPM and TRMM precipitation products using. *J Meteorol Res* 32:324–336. <https://doi.org/10.1007/s13351-018-7067-0.1.Introduction>
- Zhang Z, Tian J, Huang Y, Chen X, Chen S, Duan Z (2019) Hydrologic evaluation of TRMM and GPM IMERG satellite-based precipitation in a humid basin of China. *Remote Sens.* <https://doi.org/10.3390/rs11040431>
- Zope PE, Jothiprakash TIE (2016) Development of rainfall intensity duration frequency curves for Mumbai City, India. *J Water Resour Prot* 08:756–765. <https://doi.org/10.4236/jwarp.2016.87061>
- Zorzetto E, Marani M (2019) Downscaling of rainfall extremes from satellite observations. *Water Resour Res* 55:156–174. <https://doi.org/10.1029/2018WR022950>
- Zorzetto E, Botter G, Marani M (2016) On the emergence of rainfall extremes from ordinary events. *Geophys Res Lett* 43:8076–8082. <https://doi.org/10.1002/2016GL069445>

Publisher's note Springer Nature remains neutral with regard to jurisdictional claims in published maps and institutional affiliations.